Nuclear Instruments and Methods in Physics Research B 267 (2009) 2690–2697

Contents lists available at ScienceDirect

Nuclear Instruments and Methods in Physics Research B

journal homepage: www.elsevier.com/locate/nimb

Ion beam induced defects in solids studied by optical techniques

J.D. Comins [a,b,c,*], G.O. Amolo [a], T.E. Derry [c], S.H. Connell [c], R.M. Erasmus [b,c], M.J. Witcomb [c,d]

[a] Materials Physics Research Institute, School of Physics, University of the Witwatersrand, Johannesburg, South Africa
[b] Raman and Luminescence Laboratory, University of the Witwatersrand, Johannesburg, South Africa
[c] DST/NRF Centre of Excellence in Strong Materials, University of the Witwatersrand, Johannesburg, South Africa
[d] Electron Microscope Unit, University of the Witwatersrand, Johannesburg, South Africa

ARTICLE INFO

Article history:
Available online 9 June 2009

PACS:
61.80.Jh
61.82.−d
61.72.Ww
61.46.+w

Keywords:
Ion beams
Defects in solids
Nanoparticles
Optical techniques
Lithium niobate
Alkali iodides
Silicon
Indium tin oxide

ABSTRACT

Optical methods can provide important insights into the mechanisms and consequences of ion beam interactions with solids. This is illustrated by four distinctly different systems.

X- and Y-cut $LiNbO_3$ crystals implanted with 8 MeV Au^{3+} ions with a fluence of 1×10^{17} ions/cm^2 result in gold nanoparticle formation during high temperature annealing. Optical extinction curves simulated by the Mie theory provide the average nanoparticle sizes. TEM studies are in reasonable agreement and confirm a near-spherical nanoparticle shape but with surface facets. Large temperature differences in the nanoparticle creation in the X- and Y-cut crystals are explained by recrystallisation of the initially amorphised regions so as to recreate the prior crystal structure and to result in anisotropic diffusion of the implanted gold.

Defect formation in alkali halides using ion beam irradiation has provided new information. Radiation-hard CsI crystals bombarded with 1 MeV protons at 300 K successfully produce *F*-type centres and *V*-centres having the I_3^- structure as identified by optical absorption and Raman studies. The results are discussed in relation to the formation of interstitial iodine aggregates of various types in alkali iodides. Depth profiling of I_3^- and I_5^- aggregates created in RbI bombarded with 13.6 MeV/A argon ions at 300 K is discussed.

The recrystallisation of an amorphous silicon layer created in crystalline silicon bombarded with 100 keV carbon ions with a fluence of 5×10^{17} ions/cm^2 during subsequent high temperature annealing is studied by Raman and Brillouin light scattering.

Irradiation of tin-doped indium oxide (ITO) films with 1 MeV protons with fluences from 1×10^{15} to 250×10^{15} ions/cm^{-2} induces visible darkening over a broad spectral region that shows three stages of development. This is attributed to the formation of defect clusters by a model of defect growth and also high fluence optical absorption studies. X-ray diffraction studies show evidence of a strained lattice after the proton bombardment and recovery after long period storage. The effects are attributed to the annealing of the defects produced.

1. Introduction

The development of new forms of nuclear power reactors and the ultimate success of future fusion reactors will depend critically on a solution of a variety of materials problems associated with the radiation damage created. As examples, we may have the aggregation of primary and mobile point defects to form aggregates and clusters; extrinsic clusters can result from ion implantation and at high fluences amorphisation can occur followed by recrystallisation on heating.

Computational models exist for such processes, but the predicted intermediate stages of damage formation, cluster development, recrystallisation, etc. in many cases are not easily accessible to corroborative experimental studies. Optical spectroscopy can be useful in such situations and four examples are reviewed in the present work.

2. Lithium niobate implanted with gold ions

Lithium niobate $LiNbO_3$ (LN) has a rhombohedrally-centred hexagonal lattice and has received much attention resulting from its ferroelectric, piezoelectric, acoustic and opto-electronic properties [1]. The intrinsic and extrinsic defect structures in LN crystals have been studied extensively [2].

* Corresponding author. Address: Materials Physics Research Institute, School of Physics, University of the Witwatersrand, Johannesburg, South Africa. Tel.: +27 11 717 6812; fax: +27 11 717 6830.
E-mail address: darrell.comins@wits.ac.za (J.D. Comins).

0168-583X/$ - see front matter © 2009 Elsevier B.V. All rights reserved.
doi:10.1016/j.nimb.2009.05.074

The production of amorphised low-index near surface layers of LN by electronic excitation with high-energy ion implantation with fluences in the range $10^{10} - 10^{15}$ ions/cm^2 has been demonstrated [3]. LN implanted with various metallic ions to form metal colloids or nanoparticles has been investigated by several groups [4–6] including their non-linear properties. In particular, Rahmani et al. [4] used 360 keV Ag^+ ions with a fluence of 8×10^{16} cm^{-2} incident on the X-, Y- and Z-cut faces of LN. The directional nature of stress fields created during the implantation and the anisotropic diffusion of vacancies and interstitials were considered responsible for marked differences in the Ag nanoparticle formation on annealing the X-cut crystal as compared with the corresponding results for the Y- and Z-cut samples.

In the present work, a tandem Van de Graaf accelerator with a spatially uniform beam was used to implant 8 MeV Au^{3+} ions with a fluence of 1×10^{17} ions/cm^2 at normal incidence into X-cut and Y-cut lithium niobate (LN) specimens at room temperature (RT). SRIM2003 simulations show that the region of the vacancy distribution is uniformly amorphous due to nuclear stopping corresponding to a depth below the surface of 1.7 μm.

The implanted specimens were isochronally annealed using 30 min steps under argon gas flow at 100 K. Corrections were made to the absorption spectra resulting from the formation of oxygen vacancies on annealing [7] making use of corresponding spectra of similarly annealed virgin specimens.

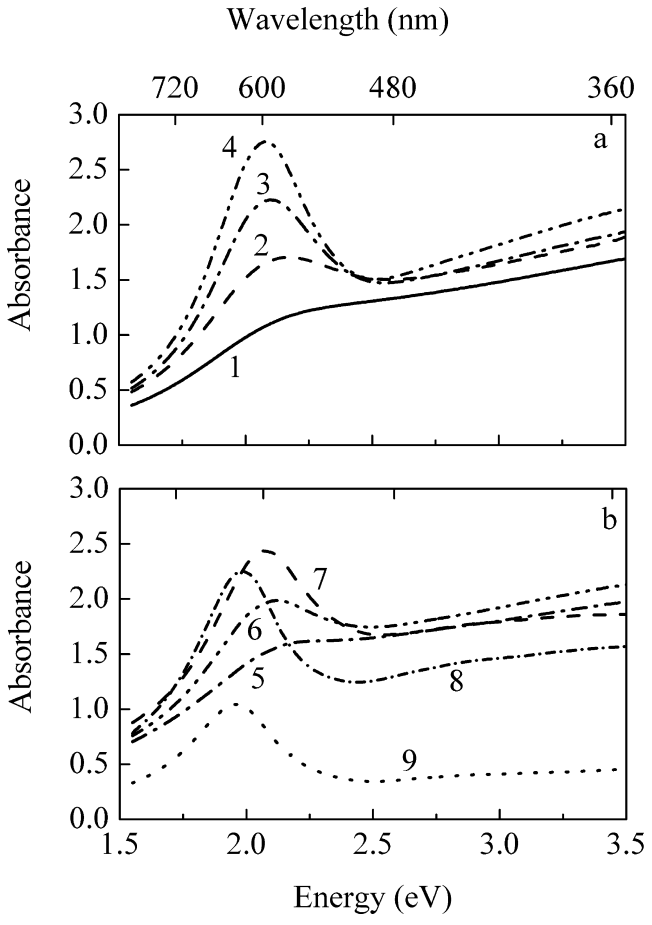

Fig. 1. Optical absorption spectra for LN specimens implanted with Au^{3+} ions with a beam energy of 8 MeV to fluences of 1×10^{17} ions/cm^2 at RT. (a) Y-cut LN after isochronal annealing for 30 min periods (1: 673, 2: 773, 3: 973, 4: 1073 K). (b) X-cut LN after isochronal annealing for 30 min periods (5: 973, 6: 1073, 7: 1173, 8: 1273, 9: 1373 K). All optical absorption measurements for figures (a) and (b) were obtained at RT.

Optical absorption spectra for Y and X-cut LN specimens each implanted at RT are shown in Figs. 1(a) and (b). The broad peak in spectrum 1 of Fig. 1(a) is found after implantation and is due to Au dimers, trimers and very small clusters [8]. The background absorption results from oxygen vacancies created during ion implantation [9] and from amorphisation for the highest fluences [6]. After annealing, an extinction band near 2.7 eV results from a surface plasmon resonance (SPR) of the Au nanoparticles [10,11]. Fig. 1(b) shows the corresponding results for the X-cut sample. For both Y- and X-cut samples, high temperature diffusion of the Au atoms leads to Ostwald ripening, resulting in a larger average nanoparticle diameter d, a sharper particle distribution and a narrower SPR peak with increasing annealing temperature. Considerably higher annealing temperatures are required to create the Au nanoparticles for the X-cut sample, while at the highest temperatures there is a substantial decrease in SPR peak height and integrated area.

For the interaction of light by very small particles, the extinction is dominated by absorption and the absorption coefficient by the Mie theory [10,11] is

$$\gamma = \frac{18\pi p \varepsilon_h^{3/2}}{\lambda}\left\{\frac{\varepsilon_2}{(\varepsilon_1 + 2\varepsilon_h)^2 + \varepsilon_2^2}\right\}.$$

$p = (N/V)\ V_o$ is the metal volume fraction, i.e. the product of the number of nanoparticles per unit volume (N/V) and their average volume V_o; ε_h is the dielectric constant of the host; λ is the wavelength of light in a vacuum. $\varepsilon(\omega) = \varepsilon_1(\omega) + i\varepsilon_2(\omega)$ is the size-dependent dielectric constant of assumed spherical metal nanoparticles. This is modified to account for diffuse scattering of electrons by their surface and can be calculated using free-electron theory also including the core electron contribution to the dielectric function [12]. The absorption has a pronounced peak corresponding to the SPR, when $[\varepsilon_1 + 2\varepsilon_h]^2 = 0$.

Fits of the Mie theory to the respective spectra shown in Fig. 1a and b for the Y- and X-cut samples were performed. An appropriate polynomial fit to the background absorption was employed in each case. Those for the X-cut sample are shown in Fig. 2. Tables 1a and b show the values of the fitting parameters for both Y- and X- samples. The shift of the peak to longer wavelength largely results from changes in ε_h. We note that crystalline LN is birefringent with an average ε_h of 5.08 [13] while amorphous LN is optically isotropic with an ε_h of 4.41 [14]. In both samples reduced values of ε_h are present in the early stages of Au nanoparticle formation corresponding to the amorphisation of the LN host and increase with higher annealing temperatures. This behaviour is attributed to the onset of recrystallisation of the host, being supported by earlier studies [15] of ion-implanted X-cut LN. The discussion follows a similar pattern for both samples except for the obviously much higher temperature for the onset of nanoparticle formation for the X-cut sample.

Since the results are more comprehensive for the X-cut sample (Table 1b) they will be examined in detail. Reduced values of ε_h are present in the early stages of nanoparticle formation namely 4.5 after the 1073 K in which recrystallisation has begun, and 4.7 after the 1173 K anneal in which recrystallisation has taken place as evidenced from electron diffraction results to be discussed later. The metal volume fraction p initially increases during annealing, since the average volume V_o of the nanoparticles increases resulting from the increase in their diameter d, provided that N/V does not decrease too rapidly. However, annealing at 1373 K results in a substantial reduction of the SPR band as a result of disassociation of the nanoparticles and dispersion of the Au atoms into the host crystal. If both melting and dispersion of the nanoparticles takes place then p will reduce since N/V and V_o will both decrease. The high values of ε_h at 1273 and 1373 K are considered due to a signif-